The Ratio of the Direct Photon Production Cross Section at 630 GeV and at 1800 GeV

Michael Strauss
University of Oklahoma, Norman, OK

DØ NOTE # 3868
May 29, 2001

Abstract

We measure the ratio of the isolated direct photon prodution cross section at $\sqrt{s} = 630$ GeV to that at $\sqrt{s} = 1800$ GeV for the central ($|\eta| < 0.9$) and forward ($1.6 < |\eta| < 2.5$) rapidity regions. We compare the result with next to leading order QCD predictions using CTEQ parton distribution functions.

1 Introduction

The results from the published Run 1A/1B direct photon cross section [2, 1] and the direct photon cross section at 630 GeV [3] are combined in this note to give the ratio of the cross sections. The measurement of the ratio is less sensitive to common systematic uncertainties and gives an important comparison between data and theoretical predictions.

2 Analysis Additions

We have made some changes in the analysis from those previously reported for the 1800 GeV and the 630 GeV results. This section describes those changes.

2.1 1800 GeV Results

The luminosity for the published Run 1A/1B cross sections is adjusted upward by 3.4% due to the E811 results.

2.2 High E_T Bins

In order to facilitate the measurement ratio in bins of $x_T = 2E_T/\sqrt{s}$, the highest E_T bins in the 630 GeV data were changed to exactly match those of the 1800 GeV data. The previous 630 GeV results had a single high E_T bin starting at $x_T = .0833$ and extending to an x_T value higher than the maximum 1800 GeV measurement. The new binning has two x_T bins with $.0833 < x_T < .0944$ and $.0944 < x_T < .1556$. For the 630 GeV data, we set the maximum E_T to be 49 GeV, or $x_T = 0.1556$, which corresponds with them maximum E_T of 140 GeV for the 1800 GeV data.

2.3 Charged Track Background

The method for determining the amount of background containing charged tracks for the 630 GeV analysis in DØ Note #3699 is different than that in the published 1800 GeV analysis. For the purposes of this ratio note we have calculated the track backgound using the same method as that used in the 1800 GeV analysis.

In the original 630 GeV analysis, the amount of background from events with charged tracks was determined by using a two step approach. First, the tracking efficiency was determined from the data using Z^0 decays. This tracking efficiency was applied to the Monte Carlo to accept events with charged tracks as good photon candidates even though a track existed in the road pointing to the photon. Therefore, the ratio of background with and without charged tracks in the Monte Carlo was determined from the Z^0 tracking efficiency and from the original ratio of charge to neutral tracks generated in the Monte Carlo. Because certain events with charged tracks were rejected in the Monte Carlo during generation, it was expected that the number of events with charged tracks in the data may be higher than that determined from the Z^0 tracking efficiency alone. Consequently, the second step in the analysis was to allow an additional contribution from events with charged tracks in the "purity" fit, essentially changing the generated ratio of background with and without charged tracks. This method should work extremely well if the actual background from events with charged tracks was *greater than or equal to* that determined from the Z^0 decays and applied to the Monte Carlo. However, if the actual background from events with charged tracks is actually *lower* than that estimated from Z^0 decays, a large systematic error may be introduced.

Therefore, we have changed the method for determing the background from charged tracks to that used in the published 1A/1B result. In this new

method, the fraction of background consisting of events with charged tracks which are not reconstructed is completely determined by the fit to the purity distribution rather than using electrons from Z^0 decays.

The purity with the new E_T bins described above, combined with fitting for the entire background from charged tracks is shown in Figs. 1 and 2 using the variable $\log(1+\log(1+E_1))$ as the discriminant in the CC and EC, respectively.

Applying the Run 1A/1B method for determining the fraction of charged track background has little effect on the final results for the CC ($|\eta| < 0.9$), but changes the results for the EC significantly as shown in Fig. 3. Each fitted purity bin in the EC has shifted to a lower value. It can be seen in Fig. 2 that signal events dominate the region at low $\log(1 + \log(1 + E_1))$, background events with charged tracks dominate the region at high $\log(1 + \log(1 + E_1))$, and neutral background events dominate the central region. When the charged and neutral backgrounds are fitted separately in the EC, the fraction of charged background events in the final sample is actually less than when that fraction is determined from Z^0 data. Because the fraction of neutral background is not constrained by the high tail (as it is when the charged and neutral background are combined into one distribution), the fit prefers a much larger fraction of neutral background, thus decreasing the fraction of signal events.

It appears that the ratio of events with charged tracks to events with neutral tracks generated in the Monte Carlo is too high. To further test this, we have fitted the purity distributions with the intial fraction of charged track background events determined from Z^0 events, but allowing the additional fraction of background events with tracks from the purity fit to be less than zero. The results of this fit are also shown in Fig. 3 (as triangles). In the EC, all of the fit points prefer a negative value for the fraction of background with tracks, except for the bin at 10.2 GeV.

The reason for the difference between the results of the method used in DØ Note #3699 and in this note is not known. We hypothesize that the tracking efficiency derived from the Z^0 data at 1800 GeV is not completely accurate at 630 GeV. If we use the parameterization for the tracking efficiency from DØ Note #3699, which is the same as that in the published Run 1A/1B paper, there are three possible reasons why there could be fewer background events in the data than in the Monte Carlo (1) if the number of tracks from the underlying event is smaller at 630 GeV than at 1800 GeV, (2) if the tracking efficiency is greater at 630 GeV than at 1800 GeV, or (3) if the conversion probability is greater at 630 GeV than at 1800 GeV. It seems that the only plausible explanation would be the first one mentioned above.

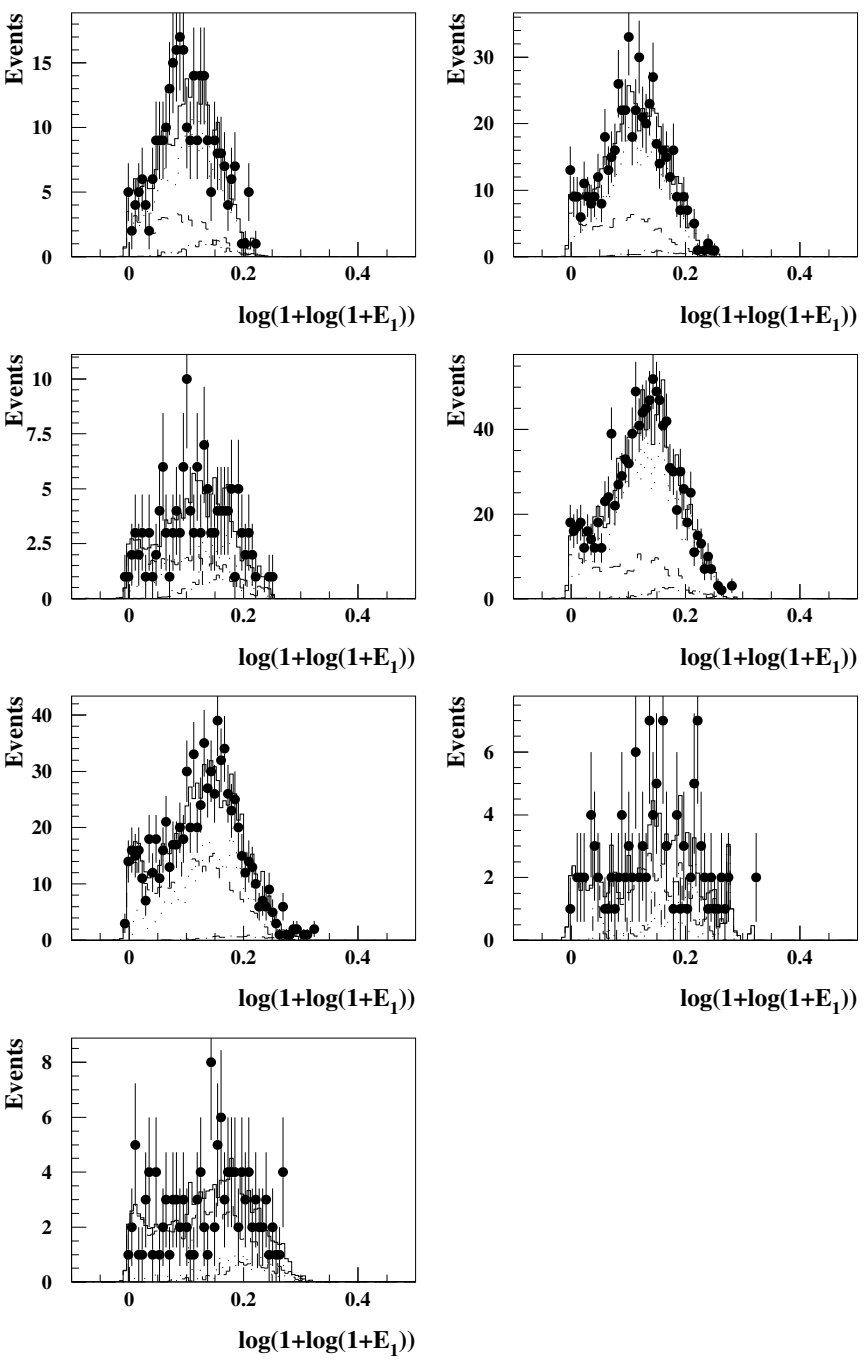

Figure 1: Distributions of $\log(1+\log(1+E_1))$ for the central η region in E_T bins of 7.35–9.10, 9.10–12.6, 12.6–14.7, 14.7–18.9, 18.9–26.25, 26.25–29.75, and >29.75 GeV. The solid line is total MC fit to the data. The dashed line is the photon contribution, the dotted line is the neutral jet background contribution, and the dash-dot line is the contribution from jets containing charged tracks.

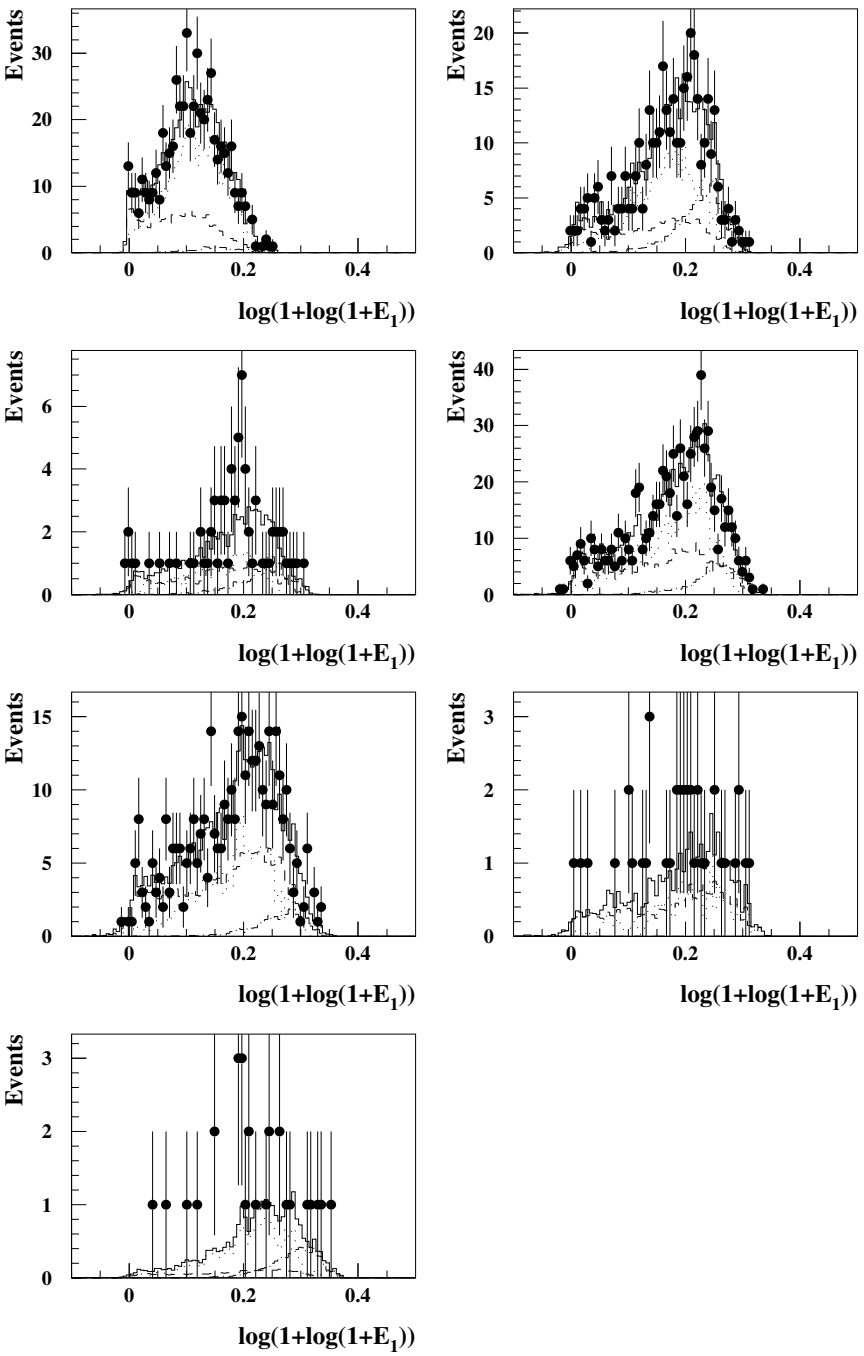

Figure 2: Distributions of $\log(1 + \log(1 + E_1))$ for the forward η region in E_T bins of 7.35–9.10, 9.10–12.6, 12.6–14.7, 14.7–18.9, 18.9–26.25, 26.25–29.75, and >29.75 GeV. The solid line is total MC fit to the data. The dashed line is the photon contribution, the dotted line is the neutral background contribution, and the dash-dot line is the contribution from jets containing charged tracks.

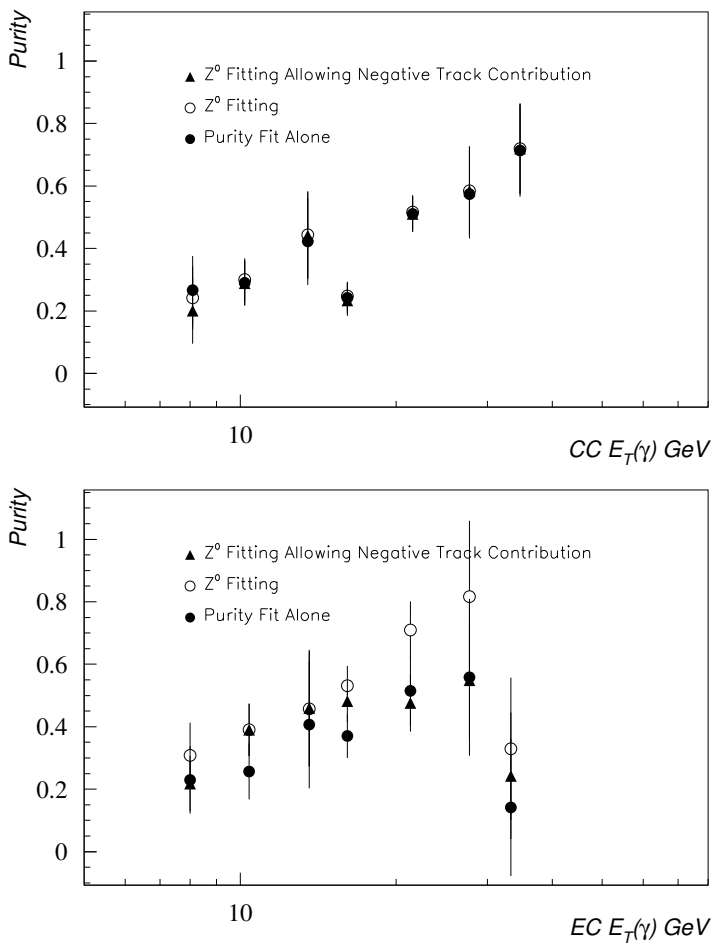

Figure 3: Photon purity using the tracking efficiency determined from Z^0 decays with extra track contributions compared to the purity with the background track contribution determined entirely from the fit. The latter method is used in the Run 1A/1B analysis, and in the revised 630 analysis in this note. The points labeled "Negative Track Contribution" are the same as the Z^0 fitting method, but allow the charged track contribution in the purity fit to be less than zero.

Although we are uncertain of the reason for the discrepency in these various methods for determining the purity, it seems that the method employed in the published Run 1A/1B analysis is the best method and is used in this analysis. The purity with the fraction of charged track background determined from the purity fit, but all other aspects of the analysis identical to that described in DØ Note #3699 is shown in Table 1 and Fig. 3. The purity divided by the efficiency is shown in Fig. 4.

E_TRange (GeV)	CC Fit	EC Fit
7.35-9.10	26.7 ± 10.9	22.9 ± 10.8
9.10-12.6	29.0 ± 7.2	25.7 ± 9.0
12.6-14.7	42.2 ± 13.9	40.7 ± 20.4
14.7-18.9	24.2 ± 4.9	37.0 ± 7.0
18.9-26.25	51.0 ± 5.7	51.5 ± 11.0
26.25-29.75	57.4 ± 14.2	53.8 ± 25.1
29.75-49.0	71.4 ± 14.8	14.2 ± 22.0

Table 1: Photon purity. In DØ Note #3699 the maximum E_T was not 49 GeV and the highest two bins in this table were a single bin.

E_T Range (GeV)	E_T	$\frac{d\sigma}{dE_T}(\frac{\text{pb}}{\text{GeV}})$	$\delta\sigma_{\text{uncor}}(\%)$	$\delta\sigma_{\text{cor}}(\%)$
7.35- 9.1	8.2	47000	43	52
9.1-12.6	10.5	7160	26	36
12.6-14.7	13.6	2040	33	25
14.7-18.9	16.5	351	22	19
18.9-26.25	22.1	131	11	13
26.25-29.75	27.9	42.6	25	10
29.25-49.0	36.9	10.5	21	7

Table 2: Differential cross section in the CC with uncorrelated and correlated errors.

2.4 Monte Carlo Energy Scale

The Monte Carlo energy scale offset is recalculated using the same method used in the 1800 GeV and 630 GeV analysis. The recalculation is necessary

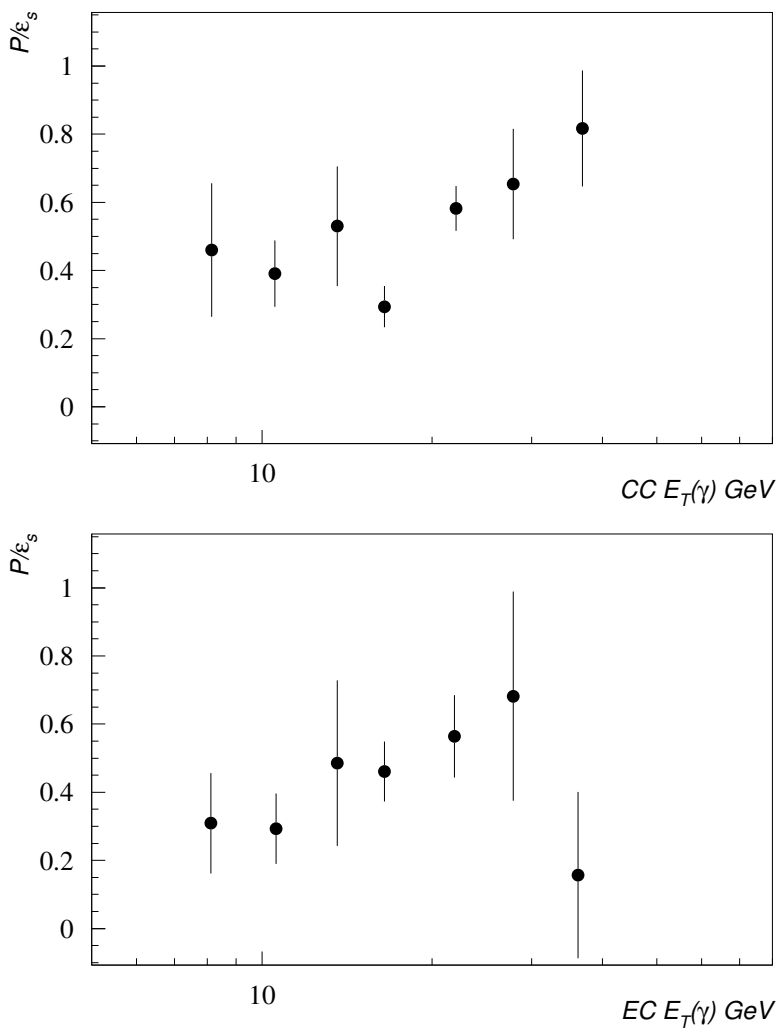

Figure 4: Photon purity divided by efficiency for the central and forward regions.

	Uncorrelated			*Correlated*				
E_T **Range**	$\mathcal{P}$	ϵ_s	**Trg**	**Frg**	**Esc**	**Act**	**Trk**	**Lum**
7.35- 9.1	41	12	6	51	6	1	2	4
9.1-12.6	25	2	6	36	5	1	2	4
12.6-14.7	33	2	1	24	3	1	2	4
14.7-18.9	20	2	8	18	3	1	2	4
18.9-26.25	11	1	1	12	2	1	2	4
26.25-29.75	25	2	0	9	2	1	2	4
29.75-49.0	21	1	0	6	2	1	2	4

Table 3: Sources of uncertainty in the CC (in percent).

E_T **Range (GeV)**	E_T	$\frac{d\sigma}{dE_T}(\frac{\text{pb}}{\text{GeV}})$	$\delta\sigma_{\text{uncor}}(\%)$	$\delta\sigma_{\text{cor}}(\%)$
7.35- 9.1	8.1	22400	48	42
9.1-12.6	10.6	3700	35	31
12.6-14.7	13.6	1170	50	24
14.7-18.9	16.5	403	20	21
18.9-26.3	21.9	67.3	22	17
26.25-29.75	27.8	16.9	45	16
29.75-49.0	36.2	0.522	160	15

Table 4: Differential cross section in the EC with uncorrelated and correlated errors.

	Uncorrelated			*Correlated*				
E_T **Range**	$\mathcal{P}$	ϵ_s	**Trg**	**Frg**	**Esc**	**Act**	**Trk**	**Lum**
7.35- 9.1	48	6	6	39	4	1	13	4
9.1-12.6	35	1	1	27	3	1	13	4
12.6-14.7	50	2	0	20	3	1	13	4
14.7-18.9	19	2	7	15	3	1	13	4
18.9-26.3	22	1	1	10	2	1	13	4
26.25-29.75	45	2	0	7	2	1	13	4
29.75-49.0	160	1	0	5	2	1	13	4

Table 5: Sources of uncertainty in the EC (in percent).

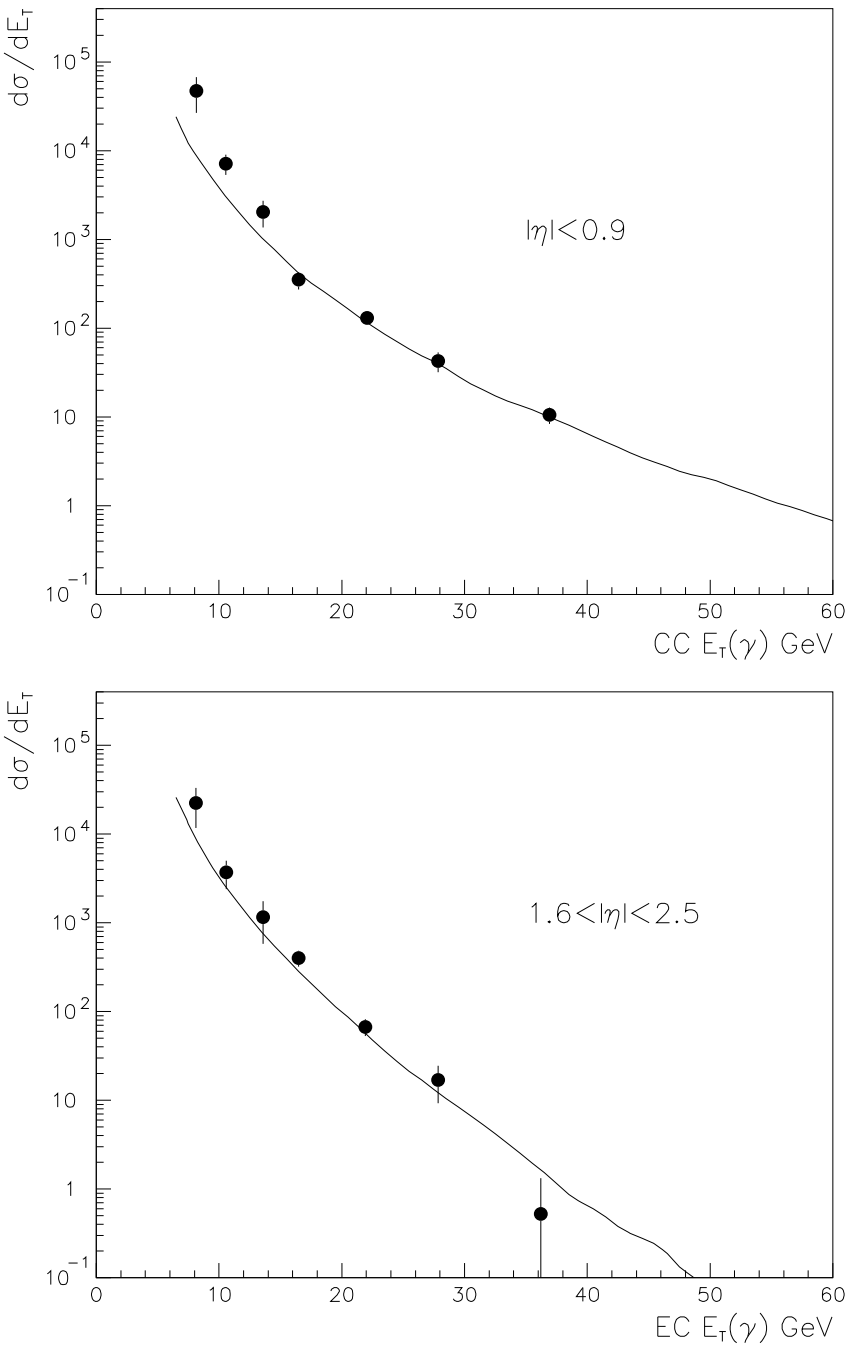

Figure 5: The isolated photon cross section, $d\sigma/dE_T\, d\eta$ vs. photon E_T for the central and forward rapidity regions. The errors are the total uncorrelated error and the curve is the theoretical prediction of CTEQ4M.

because the purity fit method has changed and the offset is determined by minimizing the global χ^2 in the purity fit. The offset is parameterized as $E_1^{MC} = \alpha + \beta E_1$. The value of β is eliminated using the $W \to e\nu$ sample so that $\beta = (E_1^{MC}(W) - \alpha)/E_1(W)$. The minimum χ^2 is found at a value of $\alpha = 60 \pm 2$ MeV. The value using the previous charged track fraction fitting method used in DØ Note #3699 was $\alpha = 62 \pm 2$ MeV.

3 Cross Section

The measured cross section is shown in Fig. 5 along with a theoretical prediction using CTEQ4M as implemented by Owens *et. al.* [4]. Fig. 6 shows the difference between the experimental and theoretical differential cross sections. The correlated uncertainty includes contributions from the uncertainty on the geometric acceptance, the luminosity, the energy scale, the tracking efficiency, and the fragmentation model. The uncorrelated uncertainty includes the uncertainties due to purity fitting (which includes statistical errors), the efficiency of the selection criteria, and the trigger efficiency. Contributions to the uncertainty from each of the sources is shown in Tables 3 and 5. The same data is plotted with the UA2 data and CTEQ5 as implemented by Vogelsang in Fig. 7 [5].

4 Significance

Both theoretical descriptions show relatively good agreement with the data. However, neither theory reproduces the data at lower E_T in the CC where the production cross section is higher than the theory.

A qualititive assessment of the agreement between data and theory is made by determining the χ^2 of the data with respect to the theory using the complete covariance matrix. For each parameter in the cross section a fractional error matrix is determined taking all correlations into account [6]. The individual correlated error matrices are added together to produce a single fractional error matrix $\boldsymbol{A}$ which contains all correlated errors for each E_T bin. The uncorrelated fractional error matrices consists of a diagonal matrix derived from the purity fit $\boldsymbol{B}$, and a diagonal matrix composed of all other uncorrelated uncertainties added in quadrature $\boldsymbol{C}$. The total error matrix ($\boldsymbol{V}$) is given by

$$V_{ij} = A_{ij}T_iT_j + B_{ij}D_iD_j + C_{ij}T_iT_j$$

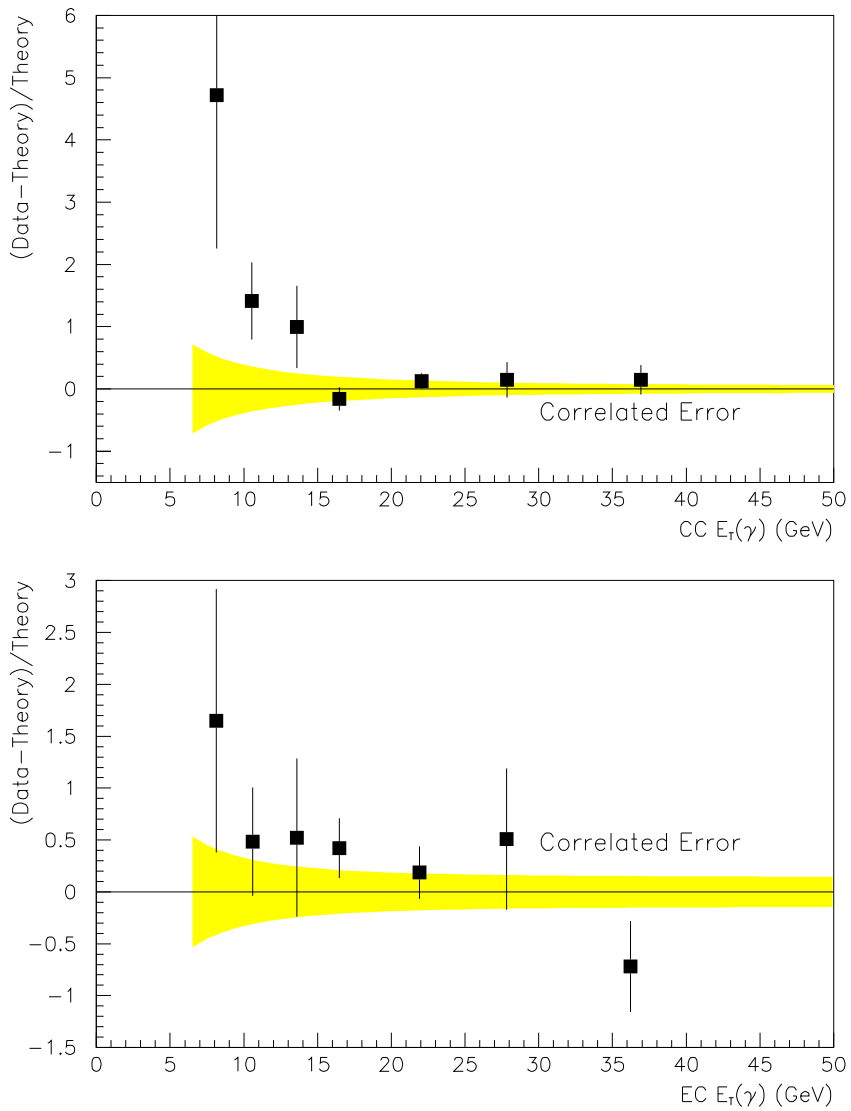

Figure 6: (Data-Theory)/Theory for the central (top) and forward (bottom) rapidity regions. The error bars indicate the uncorrelated uncertainty and the shaded region shows the correlated uncertainty.

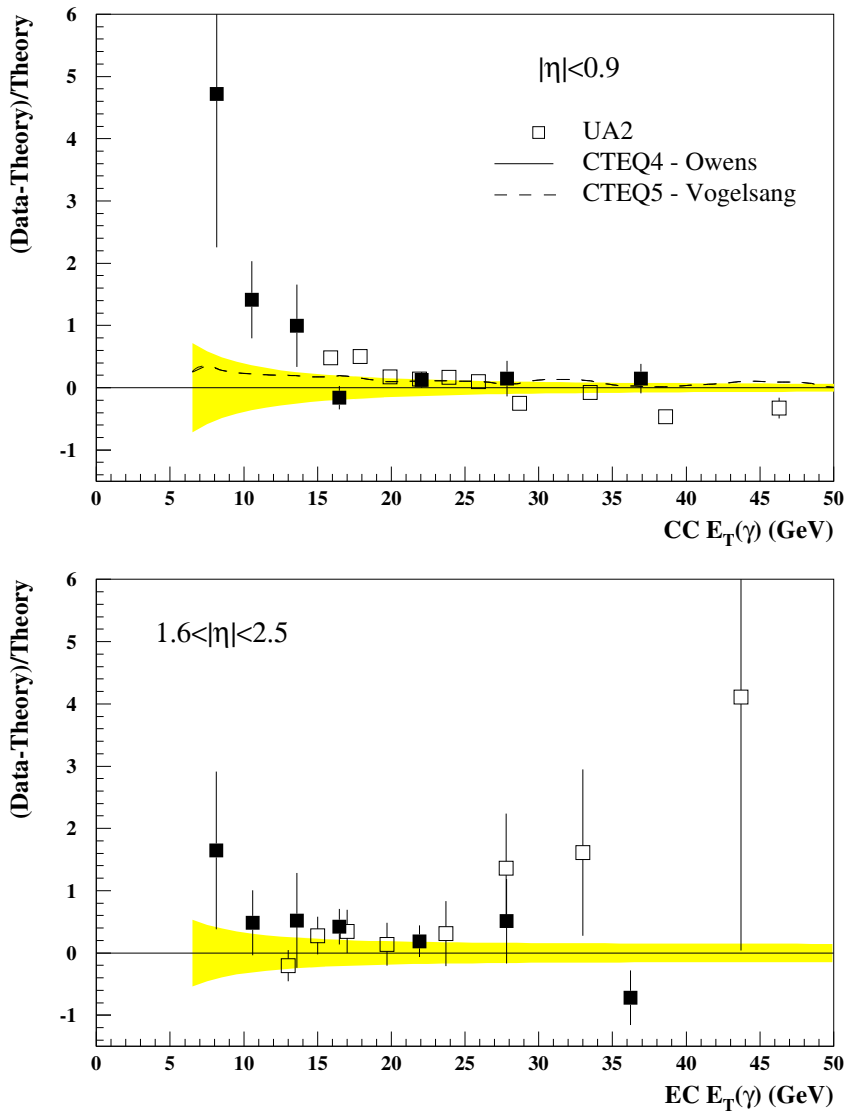

Figure 7: Same as Fig. 6 showing the UA2 data and CTEQ5 as implemented by Vogelsang. The errors for the UA2 data are statistical only, while the errors for the data in this analysis consist of all uncorrelated errors. The band shows the correlated uncertainty.

where T_i and T_j are the theoretical cross sections in the ith and jth E_T bin, D_i and D_j are the measured cross section in the E_T bins, A_{ij}, B_{ij}, and C_{ij} are the matrix elements of the matrices described above. The fractional error matrix $\boldsymbol{B}$ is scaled by the data rather than the theory because it is derived from the purity fit and is primarily dependent on the data statistics. The statistical error of the data is completely contained in the error on the purity fit and in the matrix $\boldsymbol{B}$. An overall χ^2 value is calculated using the equation

$$\boldsymbol{\chi^2 = (D - T)^T\ V^{-1}(D - T).}$$

Using the data and theory in Fig. 6 we find a χ^2 value of 11.9 (6.78) for 7 degrees of freedom in the CC (EC). Therefore, the probability that the theory fits the data is 10.4% (45.2%) in the CC (EC).

5 Cross Section Ratio

The dimensionless cross section is the spectrum of $E_T^4 \cdot E\frac{d^3\sigma}{d^3p}$ versus x_T. In collider variables this is $\frac{E_T^3}{2\pi} \cdot \frac{d^2\sigma}{dE_T d\eta}$ versus $\frac{2}{\sqrt{s}}E_T$. We calculate the ratio of the dimensionless cross sections for photon production at 630 GeV over the cross section at 1800 GeV.

5.1 Correlated Uncertainties

The correlation between the uncertainty in the luminosity at 630 GeV and at 1800 GeV has been calculated for the jet cross section measurement and is 3.4% [6]. The uncertainty on the model for fragmentation is 100% correlated since both analyses determine this uncertainty by varying the multiplicity of neutral mesons in the core of the jet by $\pm 10\%$ and use the the same Monte Carlo. The uncertainty on the tracking efficiency is 100% correlated in p_T but partially correlated in the ratio.

5.2 Uncorrelated Uncertainties

Many of the uncertainties in the cross section measurement are uncorrelated accross energy bins because they are calculated bin by bin. This includes the purity, selection efficiency, and the charged track fraction. These uncertainties may have small partial correlations across x_T bins because the same Monte Carlo distributions, (in E_T), are used in the purity fit. These

correlations are expected to be very small and are very difficult to unravel. For the purpose of this analysis, we are conservative and estimate that these uncertainties are also uncorrelated in the cross section ratio. In addition, the trigger efficiency, vertex requirement and energy scale are uncorrelated in the ratio because they are estimated using the data and the two data sets are independent.

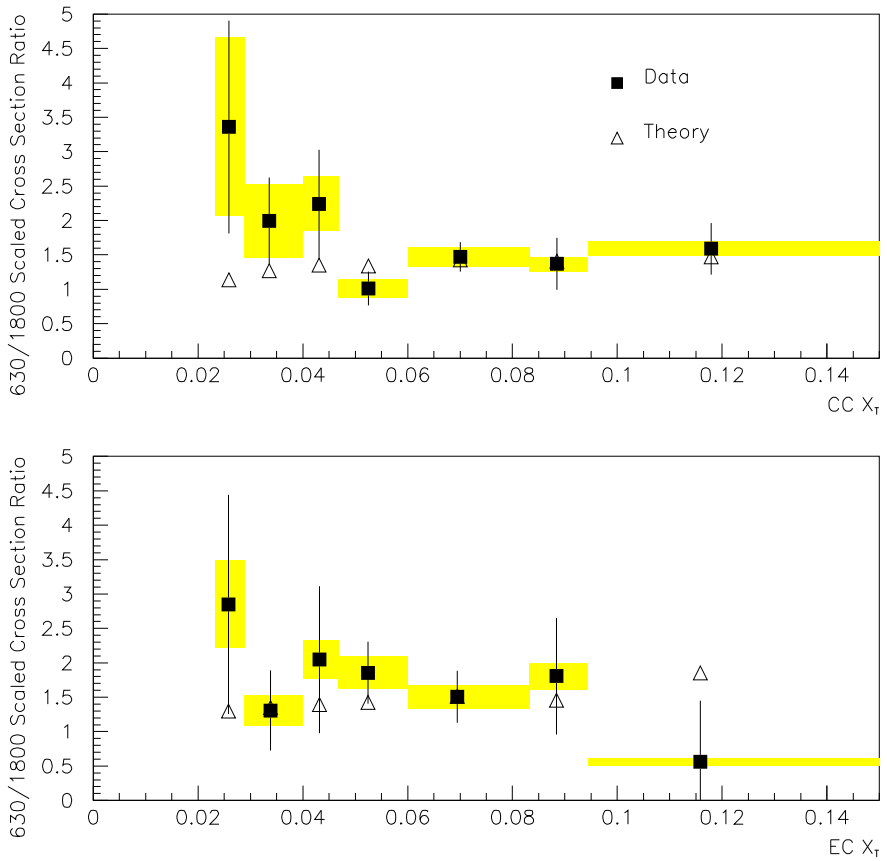

Figure 8: The ratio of the dimensionless cross section for photon production at 630 GeV to 1800 GeV. The error bars indicate the uncorrelated error and the shaded boxes indicate the diagonal terms of the correlated error matrix.

5.3 Ratio and Error Analysis

The ratio of the inclusive cross section is given by

$$R = \frac{\sigma^{630}}{\sigma^{1800}}$$

where σ represents the dimensionless cross sections in x_T for 630 and 1800 GeV. The ratio of the dimensionless cross section is shown in Fig. 8. The elements of the covariance matrix are given by

$$C_{ij} = \langle \rho_{ij} \delta R_i \delta R_j \rangle$$

with

$$\delta R_i = \frac{\partial R_i}{\partial \sigma_i^{630}} \frac{\partial \sigma_i^{630}}{\partial a} \delta a + \frac{\partial R_i}{\partial \sigma_i^{1800}} \frac{\partial \sigma_i^{1800}}{\partial a} \delta a$$

where a represents the variables that contribute to the cross section uncertainty, (e.g. purity, luminosity, etc.) and ρ_{ij} is the correlation coefficient. Completely correlated uncertainties have $\rho_{ij} = 1$ for all matrix elements and completely uncorrelated uncertainties have $\rho_{ij} = 1$ for all diagonal elements and $\rho_{ij} = 0$ for all off-diagonal elements. The elements of the complete correlation matrix are determined by summing over all of the different a variables.

The complete covariance matrix $\overline{\boldsymbol{V}}$ is composed of two matrices added together, one with correlated uncertainties and one diagonal matrix with uncorrelated uncertainties. As in Section 4,

$$\overline{V}_{ij} = \overline{A}_{ij} T_i T_j + \overline{B}_{ij} D_i D_j$$

where $\overline{A}_{ij}$ are the matrix elements of the fractional correlated uncertainties, $\overline{B}_{ij}$ are the matrix elements of the fractional uncorrelated uncertainties, and $\boldsymbol{T}$ and $\boldsymbol{D}$ are matrices with diagonal elements consisting of the theoretical and measured dimensionless cross section ratio, respectively. The purity fit is the primary contribution to the $\overline{B}_{ij}$ matrix elements. An overall χ^2 is calculated using the inverse of this error matrix as described in Section 4. We find a χ^2 value of 6.45 (4.26) for the CC (EC) for seven degrees of freedom, which gives a probability of 48.8% (74.9%) that the data and theory agree.

References

[1] "The Isolated Photon Cross Section at $\sqrt{s} = 1.8$," DØ Collaboration, *Phys. Rev. Lett.*, **84**, 2786, (2000).

[2] "The Isolated Photon Cross Section at $\sqrt{s} = 1.8$ TeV Using the Combined Run 1A/B Data Sample,"
S.L. Linn,DØ Note ♯ 3564, (1999).

[3] "A Measurement of the Isolated Direct Photon Cross Section at 630 GeV,"
M. Strauss, M. Price, DØ Note ♯ 3699, (2000).

[4] J.F. Owens, Phys. Rev, **D42**, (1990) 61.

[5] W. Vogelsang and A. Vogt, Nucl. Phys. **B453**, (1995) 334.

[6] "The Ratio of Jet Cross Sections at $\sqrt{s} = 630$ GeV 1800 GeV, DØ Collaboration, *Phys. Rev. Lett.*, to be published; "The Ratio of Inclusive Jet Cross Sections at $\sqrt{s} = 630$ GeV and $\sqrt{s} = 1800$ GeV," J. Krane, Ph.D. Dissertation, University of Nebraska, (1998).